International Journal of Nanomedicine

Dovepress
open access to scientific and medical research

Open Access Full Text Article

ORIGINAL RESEARCH

GOx-Functionalized Platelet Membranes-Camouflaging Nanoreactors for Enhanced Multimodal Tumor Treatment

Ying Du[1,2], Shujun Wang[3], Jianfeng Luan[3], Meilin Zhang[1,2], Baoan Chen[1,2,*], Yanfei Shen[2,*]

[1]Department of Hematology and Oncology, Zhongda Hospital, School of Medicine, Southeast University, Nanjing, Jiangsu, People's Republic of China; [2]School of Medicine, Southeast University, Nanjing, Jiangsu, People's Republic of China; [3]Department of Blood Transfusion, Jinling Hospital, Nanjing University School of Medicine, Nanjing, Jiangsu, People's Republic of China

*These authors contributed equally to this work

Correspondence: Baoan Chen, Department of Hematology and Oncology, Zhongda Hospital, School of Medicine, Southeast University, Nanjing, Jiangsu, 210009, People's Republic of China, Email cba8888@hotmail.com; Yanfei Shen, School of Medicine, Southeast University, Nanjing, Jiangsu, 210009, People's Republic of China, Email Yanfei.Shen@seu.edu.cn

Background: Glucose oxidase (GOx)-based starvation therapy is a new cancer treatment strategy. However, the characteristics such as limited curative effect and hypoxic tumor environment hinder its further application seriously.

Methods: Herein, doxorubicin (DOX) loaded in hollow mesoporous copper sulfide (HMCuS) nanoparticles assembled with manganese dioxide (HMMD) as nanoshell was prepared. We developed a targeted enhanced cancer treatment method to camouflage HMMD by GOx-functionalized platelet (PLT) membranes (HMMD@PG).

Results: GOx can be specially transported to the tumor site with PLT membrane for effective starvation treatment. Glucose and oxygen (O_2) in the tumor were converted to H_2O_2 under the catalysis of GOx. HMMD can catalyze H_2O_2 to produce O_2 and consume glutathione (GSH) in time, which regulates the tumor microenvironment (TME) and improves the adverse conditions of anti-tumor. In addition, DOX encapsulated in HMCuS-MnO_2 release was accelerated from the nanoparticles after the "gatekeeper" MnO_2 is consumed. The study of anti-tumor mechanism shows that the remarkable tumor suppressive ability of HMMD@PG comes from the three peaks synergy of starvation treatment, photothermal treatment (PTT), and chemotherapy. This nanoplatform disguised by PLT membrane has significant tumor inhibition ability, good biocompatibility and almost has no side effects in main organs.

Conclusion: This work broadens the application mode of GOx and shows the new development of a multi-mode collaborative processing system of nanoplatforms based on cell membrane camouflage.

Keywords: glucose oxidase, PLT membrane, nanoparticles, tumor microenvironment, tumor treatment

Introduction

Glucose is the main source of energy for tumor cell proliferation. Cancer cells mainly use glycolysis to replace the phenomenon of aerobic cycles to adapt to higher energy requirements, which is called the Warburg effect.[1] This shift to aerobic glycolysis makes cells more susceptible to cellular glucose supply, which is the principle behind cancer starvation therapy.[2] Glucose oxidase (GOx) can digest glucose to cut off the energy supply and inhibit tumor growth. This is called GOx-based starvation treatment.[3] As a natural protein oxidoreductase, GOx has the advantage of good biocompatibility. In addition, H_2O_2 produced in glucose consumption increases the level of tumor oxidative stress and can lead to apoptosis.[4–6]

However, it is challenging to block the glucose present in the tumor area due to the continuous supply of tumor blood vessels. The therapeutic effect of GOx alone is limited. Therefore, the trend of cancer treatment based on GOx has gradually changed from monotherapy to combined treatment.[7,8] Some studies encapsulated GOx in nanoparticles to achieve multimodal treatment.[9] However, most nanoparticles may still be cleared by the reticuloendothelial system (RES) during blood circulation, resulting in low targeting efficiency.[10] Another point that cannot be ignored is that solid

Received: 11 February 2022
Accepted: 13 June 2022
Published: 7 July 2022

tumors have the characteristics of hypoxia.[11] For this reason, the lack of additional oxygen (O_2) supply in the designed nanoreactor will influence the GOx mediated therapeutic effect.[12]

In this study, we demonstrated a nanoreactor that combined PLT-GOx and HMMD for the systematic treatment of tumors. Biotin modified GOx (biotin-GOx) is tightly attached to the surface of the platelet (PLT) membrane and forms PLT-GOx through biotin-protein interaction.[13] Hollow mesoporous copper sulfide (HMCuS) nanoparticles with manganese dioxide (MnO_2) nanoshell and doxorubicin (DOX) in the core were prepared (HMMD). CuS nanomaterials have the advantages of low cost, good biodegradability, and low biological toxicity. More importantly, the absorption wavelength of CuS nanoparticles is not affected by solvents and the surrounding environment, which has advantages over gold nanomaterials.[14–16] HMMD was camouflaged with PLT membrane attached with GOx for tumor treatment (HMMD@PG). Since PLTs have no cell nucleus, the collection of PLT membranes is relatively simple. Moreover, P-selectin overexpressed on the platelet membrane has an affinity with the CD44 receptor on the surface of tumor cells. As a result, the PLT membrane can target tumor actively, and the drug-loaded nanoparticles coated with PLT membrane can eliminate the uptake of macrophages and avoid complement activation, thus increasing the retention time of drugs in vivo.[17,18] After intravenous injection, PLT-GOx encapsulated nanoplatform can prolong blood circulation and promote tumor aggregation. GOx consistently consumes O_2 and glucose and produces H_2O_2 when the PLT membrane assists it in reaching the tumor tissue. This process exacerbates the hypoxia in the tumor tissue. H_2O_2 generating O_2 catalyzed by MnO_2 can solve this problem with ease. This oxygen production process lays the foundation for the continuous consumption of glucose to promote starvation treatment. Studies have shown the concentration of GSH in the tumor microenvironment is higher than that in normal tissues, which greatly enhances the risk of tumor drug resistance and metastasis.[19] MnO_2 can reduce GSH to GSSH, and MnO_2 is decomposed into Mn^{2+}. The occurrence of this series of cascade reactions not only realizes the starvation therapy but also improves the tumor microenvironment. The reaction is as follows:

$$Glu\cos e + O_2 + H_2O \overset{GOx}{\rightarrow} Gluconic + H_2O_2$$

$$H_2O_2 \overset{MnO2}{\rightarrow} H_2O + O_2$$

$$MnO_2 + GSH \rightarrow Mn^{2+} + GSSG$$

With the decomposition of MnO_2 nanoshell, DOX was released from HMCuS nanoparticles. At the same time, HMCuS can realize the function of photothermal therapy (PTT) at the tumor site under near-infrared radiation.

In conclusion, the prepared HMMD@PG can be used as a nanoreactor integrating multimodal therapy and improving the tumor microenvironment. Moreover, the copper, sulfur, and manganese contained in the nanosystem are necessary elements for human physiological metabolism, which has high safety to the human body. Therefore, the multifunctional nanoplatforms have broad applications in biomedical engineering and clinical applications.

Materials and Methods

Materials and Cells

$CuCl.2H_2O$, polyvinylpyrrolidone K30 (PVP K30), sodium sulfide (Na_2S), polyvinylpyrrolidone (PVP K30), hydrazine hydrate (50%), potassium permanganate ($KMnO_4$, 99%), methylene blue (MB, 82%), hydrogen peroxide (H_2O_2, 30%), and glutathione (GSH) were obtained from Aladdin Bio-chem Technology Co, Ltd. (Shanghai, China). Doxorubicin (DOX), glucose oxidase (GOx), biotin, 5.5'-dithiobis-(2-nitrobenzoic acid) (DTNB), and 3.5-dinitrosalicylic acid (DNS) were obtained from Macklin Bio-chem Technology Co, Ltd. (Shanghai, China). 4',6-diamidino-2-phenylindole (DAPI), and Cell Counting Kit-8 (CCK-8) were obtained from Beijing Solarbio Technology Co, Ltd. (Beijing, China). Glucose oxidase Kit was obtained from (Jining, Shanghai, China). Dulbecco Minimum Essential Medium (DEME) was provided by Gibco Invitrogen Corp. The platelet was supplied by the Chinese Red Cross within 5 days of drawing blood. All other chemical reagents were analytically pure and used directly as received.

Murine breast cancer cell (4T1) was obtained from the National Collection of Authenticated Cell Cultures (Nanjing, China). 4T1 cells were cultured in a DEME medium with 10% FBS. The cells were incubated in a humidified and normoxic atmosphere with 5% CO_2 at 37 ◦C.

Preparation of PLT Membrane

PLT membrane was derived by a repeated freeze-thaw process. Aliquots of PLT suspensions were first frozen at −80 °C, and thawed at room temperature. After eight times of repeated freezing and thawing, the PLT was centrifugated at 12,000 rpm for 5 min. Following three repeated washes with phosphate buffered saline (PBS) solution mixed with protease inhibitor tablets, the pelleted PLT membranes were suspended in water and sonicated in a capped glass vial for 5 min using a KQ-400KED bath sonicator at a power of 80 W. The presence of PLT membrane vesicles was verified by morphological examination by transmission electron microscopy (TEM, FEI, US).

GOx Connected to PLT Membrane (PLT-GOx)

To obtain the biotinylated GOx, 10 mg of biotin was dissolved in 1 mL of dimethylformamide, and then immersed in 5 mL of GOx solution (2 mg/mL) for 60 min with the presence of N, N-carbonyldiimidazole at room temperature. Afterward, the resultant solution was subjected to dialysis against deionized water for 24 h (14 kDa molecular cut-off). To optimize the proportion between biotin-GOx and PLT membrane, different amounts of biotin-GOx were transferred into the PLT membrane solution for 2 h at 4 °C. Finally, PLT-GOx were obtained by centrifugation and washed thrice using PBS to remove unconjugated GOx. The GOx concentration was detected by glucose oxidase test kits.

Synthesis of Mesoporous Copper Sulfide Nanoparticles (HMCuS)

480 mg of PVP-K30 was dissolved in 50 mL of water. 200 μL $CuCl_2.2H_2O$ solution (0.5 mol/L) was added to PKP-K30 solution and stirred for 5 min. 50 mL aqueous solution (pH = 9) and 12.8 μL 50% hydrazine hydrate were added to the stirred $CuCl.2H_2O$ solution. After stirring the above solution for 5 min, add 400 μL Na_2S solution with a concentration of 320 mg/mL. The mixed solution was stirred in an oil bath at 60°C for 2 h. After the reaction, the precipitate was obtained by centrifugation. The HMCuS nanoparticles were obtained by washing with ultrapure water until neutral and drying.

Synthesis of DOX Loaded HMCuS

HMCuS (10 mg) was dissolved into PBS (10 mL). Afterward, DOX (1.0 mg) was added, and then the mixtures were stirred in the dark at 25 °C for 24 h. Finally, the product was centrifuged at 11,000 rpm for 6 min and then washed with deionized water two times. The above product was dissolved in PBS or freeze-drying for future use. The loaded capacity of DOX was measured according to their absorption peaks at 480 nm in the UV–vis spectrum. The loaded amount of DOX was calculated by the concentration difference between before and after loading. The encapsulation efficiency (EE) of DOX in HMCuS was calculated as follows:

$$EE(\%) = \text{Weight of loaded DOX} \,/\, \text{Weight of feeding DOX} \times 100\%$$

Preparation for HMCuS-DOX-MnO_2 (HMMD)

HMCuS-DOX (10 mg) was dissolved into deionized water (25 mL). Next, the $KMnO_4$ aqueous solution 2 mL, 10 mg/mL was added dropwise to the HMCuS-DOX solution under the ultrasonic processing, followed by a reaction for 20 min. Subsequently, the above mixtures were immediately collected by centrifugation at 10,000 rpm for 5 min. Finally, the product was washed with deionized water three times and freeze-drying.

PLT-GOx Coated Nanomaterials (HMMD@PG)

PLT-GOx cloaking was then accomplished by dispersing and fusing 1mL PLT-GOx membrane vesicles with 2 mg HMMD via sonication using a bath sonicator at a frequency of 100 W for 5 min. The diameter and the surface zeta

potential of the replicate HMMD@PG samples (n=3) were obtained by dynamic light scattering (DLS) measurements using a Malvern Zetasizer Nano ZS90 (Britain).

Catalytic Reactions of HMMD@PG

Dinitrosalicylic acid (DNS) was used for the detection of glucose consumption.[20] Briefly, glucose solution in PBS (5 mL, 2 mg/mL, pH 7.4) was added to HMMD@PG solution (5 mL). The concentration of GOx is 16 μg/mL in the mixed solution. At the predetermined time intervals, a tiny solution (0.5 mL) was withdrawn and incubated with 1.5 mL DNS at 100 ◦C for 5 min. Enzyme-labeled instrument (Thermo Fisher Scientific, USA) was employed to monitor the absorbance at 450 nm, and the glucose consumption was determined according to the standard curve.

In addition, the dissolved oxygen produced by HMMD@PG (0.2 mg/mL) in the glucose solution (2 mg/mL) was monitored using a portable dissolved oxygen meter (JPBJ608 Leici, Shanghai). The concentration of H_2O_2 was detected by the ammonium molybdate method. H_2O_2 reacted with ammonium molybdate to form a complex, and the OD value was determined at 405 nm.

H_2O_2 Content (mmol/L) = (experimental group OD value - Blank OD value)/(standard OD value - Blank OD value) × Standard concentration × Sample dilution ratio.

GSH Depletion by HMCuS-MnO_2

Different concentrations of GSH (0 and 2 mM) were incubated with HMCuS-MnO_2 solution ([Mn] =0.13 mM) at 37 °C for 30 min. The unreacted GSH was indicated by DTNB via UV-vis spectra.

Similarity, Different concentrations of HMCuS-MnO_2 (0, 100, 200, and 400 μg/mL) were incubated with GSH solution (2 mM) at 37 °C for 30 min. The unreacted GSH was indicated by DTNB via UV-vis spectra.

DOX Release

The release of DOX were monitored based on the intensity of UV–vis absorption in the supernatant. Typically, HMMD@PG was added into PBS solution with different pH, PBS solution containing GSH, and PBS solution containing GSH with NIR light irradiation. Subsequently, the mixed solution was transformed into dialysis bags (MWCO: 1000 Da) and immersed in PBS (pH 7.4). Then, the solution was incubated at 37 °C. At regular intervals, 2 mL of supernatant were taken out and replaced. The releasing efficiency of DOX was determined according to the calibration curve of DOX.

Photothermal Properties and Photothermal Conversion Efficiency (η) of HMMD@PG

To investigate the photothermal properties of the nanoparticles, different concentrations of HMMD@PG (0, 25, 50, 100, and 200 μg/mL) solution were exposed to near-infrared (NIR) laser (808 nm, 1.5 W/cm^2) for 8 min. To investigate the relationship between the photothermal effects and laser power, HMMD@PG (100 μg/mL) solution were irradiated at 0.5, 1.0, 1.5, and 2.0 W/cm^2 for 8 min. The photothermal stability of HMMD@PG suspension was investigated under NIR irradiation for four on−off cycles. The suspension temperature was measured at 30s intervals and recorded by a thermal imaging camera (Hti HT19, China) under NIR irradiation.

To examine the photothermal effect of HMMD@PG, the photothermal conversion efficiency was calculated according to the following equation:

$$\eta = \frac{hs(T_{max} - T_{surr}) - Q_{dis}}{I\left(1 - 10^{-A808}\right)}$$

The T_{max} means the equilibrium temperature of HMMD@PG. T_{surr} is ambient temperature of the surroundings. The Q_{dis} is heat loss from light absorbed by the container, I is the laser power (1.5 W/cm^2). $A808$ is the absorbance value of HMMD@PG at 808 nm.[21]

Targeted Recognition and Cells Internalization

4T1 cells were seeded in 15 mm confocal dishes with the density of 1×10^6 cells per well and incubation for 12 h. The HMMD (DOX = 4 μg/mL) and HMMD@PG (DOX = 4 μg/mL) were added into the confocal dishes to culture with cells

for different times. The treated cells were washed three times with PBS and stained with the DAPI (Ex/Em = 359/461 nm) for 5 min. Then, the treated cells were fixed with 4% polyformaldehyde and washed with PBS. At last, the cells were observed under the confocal laser scanning microscope (CLSM).

Intracellular Hypoxia Detection

The Hypoxia Detection Kit was used to analyze the intracellular hypoxia induced by GOx. Briefly, 4T1 cancer cells were inoculated into 15 mm confocal dishes at a cell density of 1×10^6 cells per well and incubated for 12 h to allow the attachment of cells. Then, the cells were incubated with free GOx (16 μg/mL), HMMD (200 μg/mL) and HMMD@PG (HMMD = 200 μg/mL, GOx = 16 μg/mL) for 4 h. The same volume of PBS served as a control. Hypoxic fluorescence probes were added to each cell culture media, respectively. And measured them using CLSM. (Green: Ex/Em = 536/610 nm).

The Generation of ROS in Cells

To verify the generation of ROS in cells, 1×10^6 4T1 tumor cells were separately cultured in 15 mm confocal dishes and treated with PBS, HMCuS-MnO_2, HMCuS-MnO_2 @PG, and HMCuS-MnO_2@PG + L (Laser) (HMCuS-MnO_2 =200 μg/mL). After the co-incubation at 37 °C for 4 h, the free samples were washed out. HMCuS-MnO_2@PG + L group irradiated by the 808 nm laser (1.5 W/cm^2, 5 min). Singlet oxygen probe DCFH-DA (10 μM, λex = 488 nm, λem = 525 nm) was added to incubate with the cells for 20 min. The cell medium was discarded and rinsed with PBS twice. The fluorescence of DCF was detected by CLSM.

Cell Viability Test

4T1 cells were seeded in 96-well plate at a density of 1×10^5 cells per well in 100 μL DMEM with 10% FBS at 37 ◦C with 5% CO_2 humidified atmosphere. After 12 h incubation, the medium was changed with fresh DMEM, and cells were treated with DOX, HMMD, HMMD@PG, and HMMD@PG + L (808 nm 1.5 W/cm^2 5 min). The concentration gradient of DOX was consistent in each treatment group (DOX=0.5 μg/mL, 1 μg/mL, 2 μg/mL, 4 μg/mL and 8 μg/mL). The concentration of Gox was 0.54 μg/mL, 1.08 μg/mL, 2.16 μg/mL, 4.32 μg/mL and 8.64 μg/mL respectively. After incubation for 4 h, the free samples were washed out then continued incubation for 20 h. CCK8 assay was employed to estimate the cell viability. Finally, the absorbance at 450 nm was measured by the enzyme-labeled instrument. The relative cell viability was calculated as (OD450 sample/OD450 control) ×100%, and all experiments were performed in triplicate.

Live/Dead Cell Staining Assay

4T1 cells were incubated in the 15 mm confocal dishes with the density of 1×10^6 cells per well and cultured in a 1 mL DMEM medium. After 12 h, the cells were treated with DOX, HMMD, HMMD@PG, HMMD@PG + L (808 nm 1.5 W/cm^2 5 min). The concentration of DOX and GOx is 4 μg/mL and 4.32 μg/mL, respectively. Furthermore, the cells without any treatments were used as a control. After incubation for 12 h, the culture medium was abandoned and washed with PBS. Then, these treated cells were stained with 100 μL Calcein-AM/PI (Calcein-AM=2 μM, PI=4.5 μM) and incubated for 15 min at 37°C. Finally, the cells were washed with PBS 3 times and analyzed with the CLSM (Calcein-AM: Ex/Em = 490/515 nm, PI: Ex/Em = 535/617 nm).

Animal Experiments

Healthy male nude mice (4–5 weeks of age) were purchased from the Changzhou caverns laboratory animal Co, Ltd. All animal experiments complied with the National Institutes of Health guide for the care and use of laboratory animals (NIH Publications No 8023, revised 1978). Ethics approval was received from the Medical Ethics Committee of Zhongda Hospital, Southeast University (Reference number: 2021ZDKYSB118).

Tumor Model: The cultured mice breast cancer 4T1 cell (1×10^6) suspension was collected and inoculated subcutaneously in the right flank abdomen of nude mice to generate tumors. The transplanted tumor size was monitored by a vernier caliper and the tumor volume (V) was calculated as $V = 1/2\times a\times b^2$, where a and b were the length and width of the tumor, respectively.

In vivo Bioluminescence and Imaging

Bioluminescence images were collected with a Xenogen IVIS Spectrum Imaging System (PerkinElmer, US). 4T1 tumor-bearing nude mice were intravenously injected with ICG and HMCuS-ICG-MnO_2@PG. The ICG concentration was consistent between the two injected groups of mice (100 μg/mL, 200 μL). The distribution of fluorescence in vivo was observed by the imaging system after 0 h, 1 h, 4 h, 12 h, 24 h, and 48 h, respectively. The excitation wavelength was fixed at 765 nm, while the emission wavelength was set to 800 nm via a filter. The exposure time of 100 ms was used for each image frame.

In vivo Anti-Tumor Evaluation

When the tumor volume reached 80 mm^3 approximately, 4T1 cancer-bearing nude mice were randomly divided into 5 groups (5 mice in each group). The mice were treated with PBS, DOX, HMMD@PM, HMMD@PG and HMMD@PG + L (808nm, 1.5W/cm^2, 10min) via tail intravenous injection every 2 days for 3 times. The doses of DOX and GOx were 5 mg/kg and 5.4 mg/kg, respectively. The tumor volumes and body weights were measured every other day. All mice were euthanized, and the tumor tissues and major organs were collected for histological analysis after 14 days.

Statistical Analysis

All data were shown as means ± standard deviation (SD). The comparison of two groups was performed by Student's *t*-test. Asterisks indicated significant differences (*$P < 0.05$, **$P < 0.01$, ***$P < 0.001$, ****$P < 0.001$). *$P < 0.05$ was considered to be statistically significant.

Results and Discussion

Characterization of PLT Membranes and PLT-GOx

PLT membranes were processed for nanoparticle cloaking. The PLT was prepared into PLT membranes by the method of repeated freeze and thawing. TEM showed that the diameter of the PLT membrane was about 200 nm (Figure 1A). The

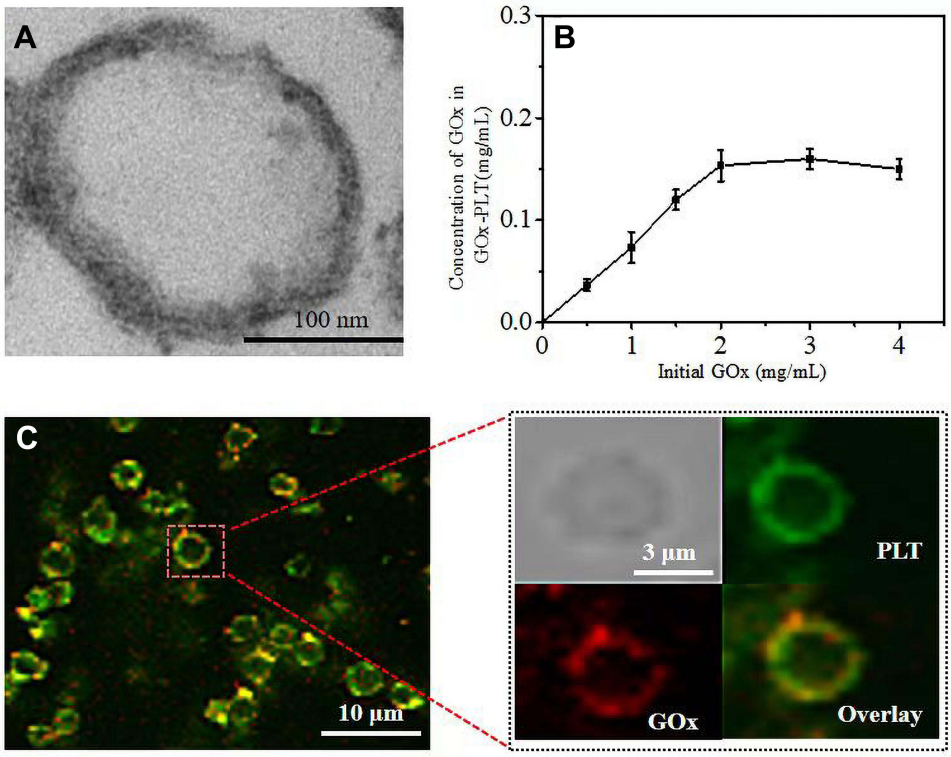

Figure 1 (**A**) TEM images of PLT membrane stained with uranyl acetate. Scale bar = 100 nm. (**B**) Relationship between initial GOx concentration and the concentration of GOx on the PLT-GOx. (**C**) CLSM images of PLT-GOx, DiD-labeled PLT (green), and rhodamine B (red)-modified biotin-GOx were used to fabricate PLT-GOx.

modification of GOx on the surface of PLT membrane to realize the glucose-responsive property is essential in this work. Thus, biotinylated GOx was anchored to the surface of PLT through a strong affinity between protein and biotin. To facilitate CLSM visual observation, we attached GOx to the surface of PLTs before they were repeatedly frozen and thawed. As shown in Figure 1C, DiD-labeled PLT membranes could be observed (shown in green color). With close observation, weak red color (rhodamine B-labelled GOx) was located on the PLT membranes. In the overlay image, we could see that the DiD-PLT were covered with a layer of rhodamine B (red)-labeled GOx, which confirmed the anchoring of GOx on the surface of PLT membranes. Next, we studied the effects of different concentrations of GOx on the attachment of GOx to the PLT membrane. A positive correlation was found between the amount of GOx on the PLT membrane, and the amount of GOx added in the reaction. The amount of connection approached the maximum when the added concentration of GOx reached 3 mg/mL (Figure 1B).

Characterization of HMMD@PG

HMCuS in our work was prepared according to previous reports with slight modifications.[15,16,22] The HMCuS was prepared by sacrificial template chemical conversion method based on Kirkendall effect. The reaction mode in the preparation process is as follows:

$$4Cu^{2+} + 8OH^- + N_2H_4 = 2Cu_2O + 6H_2O + N_2 \quad (1)$$

$$2Cu_2O + 4S^{2-} + O_2 + 4H_2O = 4CuS + 8OH^- \quad (2)$$

Where Cu_2O was used as the template and was transformed into a shell through the chemical reaction on its surface. Meanwhile, the core was removed by Kirkendall diffusion. It should be noted that no special process was required to modify the template surface and remove the template core. TEM shows the uniform hollow and mesoporous morphology of the HMCuS with an average diameter of about 154.17 nm (Figures 2A and S1A). After DOX loading, it can be observed that the hollow structure of HMCuS is not clear as before (Figure 2B). The average diameter of HMCuS-DOX is about 178.6 nm (Figure S1B). In general, MnO_2 was generated from a simple redox reaction between $KMnO_4$ and the CuS under ultrasonic conditions, where Mn^{7+} was reduced by S^{2-}, forming Mn^{4+}. The amine functional group on HMCuS-DOX interacts with Mn (HMCuS-DOX-MnO_2) to form a stable coordination covalent bond.[23] As Figure 2C show, the surface the HMCuS becomes uneven after MnO_2 nanoshell wrapped in HMCuS-DOX. The coating of the MnO_2 enlarges the average diameter of the HMMD to about 189.8 nm (Figure S1C). As observed in Figure 2D–G, the elemental mapping showed a wide distribution of the elements such as Cu, S, O,

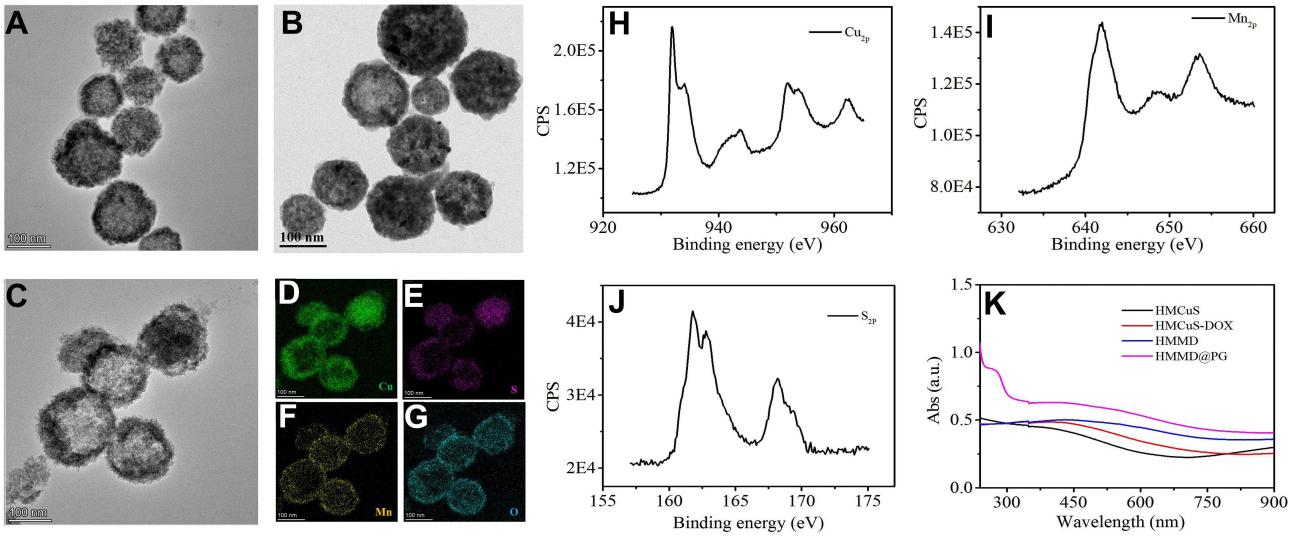

Figure 2 (**A**) TEM images of HMCuS, (**B**) HMCuS-DOX and (**C**) HMMD nanoparticles. (**D–G**) EDS elemental mapping of HMMD. ((**D**) Cu element (green color), (**E**) S element (purple color), (**F**) Mn element (yellow color), (**G**) O element (blue color)). (**H**) XPS of Cu_{2p}, (**I**) S_{2p}, and (**J**) Mn_{2p} raised from HMMD nanoparticles. (**K**) UV–vis absorption spectra of HMCuS, HMCuS-DOX, HMMD and HMMD @PG.

and Mn in the HMCuS materials. The mass ratio of Cu/Mn is 8: 1 (Table S1), which was obtained from the energy-dispersive X-ray spectroscopy (EDS) analysis. X-ray photoelectron spectroscopy (XPS) was further measured for element analysis (Figure 2H–I). The binding energy peaks at 933.08 eV and 942.68 eV are attributed to the Cu $2p_{3/2}$, and the peaks at 953.18 eV and 962.28 eV are contributed to the Cu $2p_{1/2}$.[15] Besides, the peak at 161.78 eV corresponds to S 2p.[24] The formation of MnO_2 was further supported by the XPS analysis. As shown in Figure 2J, the Mn $2p_{1/2}$ peak at 653.58 eV and Mn $2p_{3/2}$ peak centered at 641.88 eV could be assigned to a +4 state of Mn.[25] The characteristic absorption located within NIR region from 700 to 900 nm is observed from the UV-vis-NIR absorption spectrum of HMMD (Figure 2K), making it possible for PTT. Successful cloaked HMMD by PLT-GOx was also demonstrated. The wrapping of the PLT-GOx membrane expands the average diameter of HMMD to about 289.23nm (Figure S1D). The presence of PLT-GOx on the HMMD surface rendered the conjugate negatively charged and endowed it with higher in vivo biocompatibility (Figure S2A).

In vitro Catalytic Performance

As an endogenous oxidoreductase, GOx can convert intratumoral glucose and O_2 into gluconic acid and H_2O_2 effectively.[4] The catalytic activity of GOx in HMMD@PG can be monitored according to the changes in glucose and H_2O_2 concentration during glucose oxidation. As shown in Figure 3A and B, the concentration of glucose and H_2O_2 were obviously decreased and increased

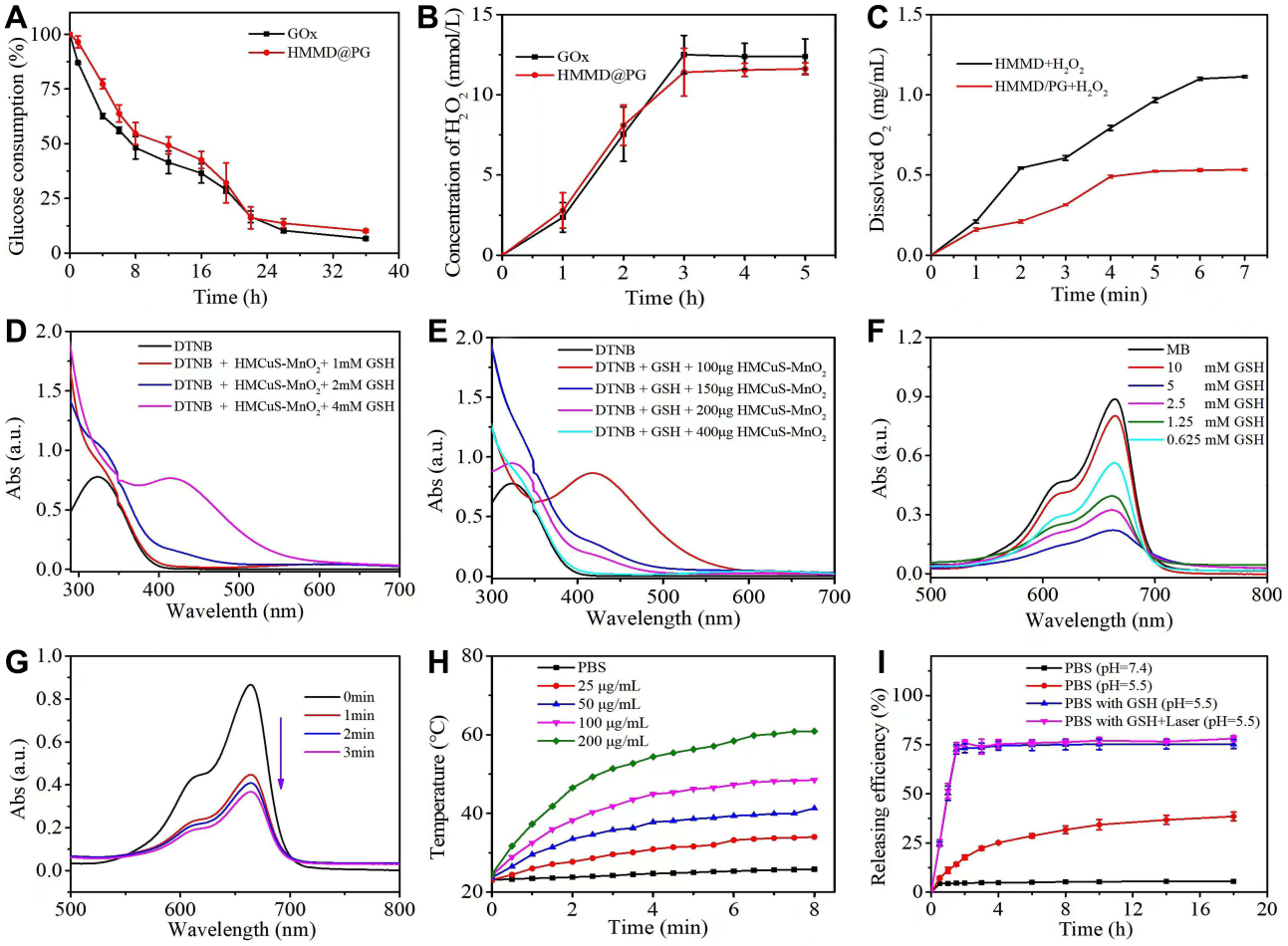

Figure 3 (**A**) Time-dependent glucose consumption in the PBS (0.01 M, pH = 7.4) solution containing 1 mg/mL of glucose and 16 μg/mL of GOx. (**B**) Time-dependent H_2O_2 generation in the PBS (0.01 M, pH = 7.4) containing 1 mg/mL of glucose and 16 μg/mL of GOx concentration. (**C**) Dissolved O_2 generation kinetics of HMMD and HMMD@PG in the PBS (0.01 M, pH = 7.4) solution. (**D**) UV–vis spectra of DTNB, DTNB + GSH, and DTNB + GSH + HMCuS-MnO_2 after 30 min of incubation. (**E**) UV–vis spectra of DTNB, DTNB + GSH, and DTNB + GSH containing different concentrations of HMCuS-MnO_2 after 30 min of incubation. (**F**) UV–vis spectra of MB in the PBS (0.01 M, pH = 7.4) solution after the addition of HMCuS-MnO_2, GSH and H_2O_2. (**G**) UV–vis spectra of MB in the PBS (0.01 M, pH = 7.4) solution in the presence of HMCuS-MnO_2, GSH and H_2O_2 after NIR laser irradiation (1.5 W/cm^2, 808 nm) for different time. (**H**) Photothermal conversion curves of a suspension of the HMMD@PG with various concentrations under NIR laser irradiation (1.5 W/cm^2, 808 nm) for 8 min. (**I**) DOX release profiles of HMMD@PG under different conditions.
Abbreviations: PBS, phosphate buffered saline; DTNB, 5,5'-dithiobis-(2-nitrobenzoic acid); GSH, glutathione; MB, methylene blue.

respectively after GOx, and HMMD@PG were added to the glucose solution. The change in glucose concentration is calculated according to the standard curve established by DNS colorimetry (Figure S3A). The results indicated that the GOx in HMMD@PG also had good biological activity compared to the free GOx that can promote the catalytic reaction. Glucose consumption by GOx is an oxygen-consuming process. However, the hypoxic state of the tumor microenvironment (TME) will limit a series of responses caused by GOx. Therefore, MnO_2 introduced on the HMMD can catalyze H_2O_2 to produce O_2. The generation of dissolved oxygen increased significantly when HMMD was added to the solution containing H_2O_2 (Figure 3C). In the HMMD@PG group, the dissolved oxygen generation decreased slightly due to the oxygen consumption by GOx.

GSH Depletion and •OH Generation

The TME is characterized by hypoxia and high concentration of GSH.[19] Studies have shown that the increase of GSH level in TME can make tumor cells resistant to chemotherapeutic drugs and promote tumor metastasis.[26] The GSH can reduce MnO_2 in HMMD to Mn^{2+}. This process consumes GSH via Equation 1, which is beneficial for improving the tumor microenvironment. DTNB was selected as an indicator of GSH.[4] The GSH can react with DTNB and the resulting 5 - thio-2 - nitrobenzoic acid (TNB) shows absorption peak at 412nm. It can be seen that when the prepared nanoplatform consumed GSH, the absorption peak of TNB at 412nm decreased significantly.(Figure 3D). Similarity, More GSH was consumed as the increased amount of MnO_2 in the solution (Figure 3E). Whereafter, GSH-activated chemo-dynamic efficacy was studied. MB was selected as the indicator of ·OH. The ·OH reacted with MB, resulting in a reduced absorption peak of MB at 665 nm.[27,28] As exhibited in Figure 3F, the UV–vis absorption spectra of MB were detected in the mixed solution of HMMD@PG, H_2O_2, and GSH. MnO_2 oxidizes GSH to GSH disulfide (GSSG), which promotes the formation of ·OH via Equation 2. In a specific range of GSH concentrations, the degradation of MB increased with the increase of ·OH production. However, due to the clearance effect of excessive GSH on ·OH, MB degradation is negligible at high concentrations of GSH (10 mM).[28] Notably, the degradation rate of MB under NIR (808 nm, 1.5 W/cm^2, 2 min) was 2.3-fold in the solution of H_2O_2 (1 mM) and GSH (10 mM) -treated HMMD (Figure 3G) compared with the no irradiation-treated group. This phenomenon proved that the level of ROS could be enhanced under NIR irradiation.

$$MnO_2 + GSH \rightarrow Mn^{2+} + GSSG \tag{1}$$

$$H_2O_2 \xrightarrow{Mn^{2+}/HCO^{3-}} \bullet OH + OH^- \tag{2}$$

Photothermal Performance and Drug-Releasing

In the as-prepared HMMD@PG nanoplatform, the HMMD played a critical role not only in promoting cascade reaction but also for photothermal performance, thanks to its excellent photothermal conversion efficiency in NIR region. The increase in temperature is positively correlated with the concentration of HMMD@PG and irradiation power (Figures 3H and S4A). No noticeable temperature change is detected in PBS free of the nanoplatforms. After four cycles of heating and cooling, the temperature of the HMMD@PG solution can still reach about 50°C (Figure S4B). This result shows that the prepared nanoplatform has excellent light and thermal stability. The corresponding photothermal conversion efficiency was 28.59% (Figure S4C-D).

The standard UV–vis adsorption curves of different concentrations of DOX in deionized water and the corresponding standard calibration curve are shown in Figure S5A. The value of best EE was calculated to be about 73.67% ± 2.44% based on the UV–vis absorption spectra of supernatant during the preparation of HMMD (Figure S5B). To validate the release efficiency of the drug, the HMMD@PG were dissolved in diverse PBS solutions by changing the two factors of GSH amount and pH value (Figure 3I). MnO_2 nanoshell stays stable in PBS (pH 7.4) free with GSH and prevents the release of DOX from the HMMD. Only 35% of DOX is then released within 8 h when the nanosystem in PBS with pH=5.5. As previously mentioned, the tumor microenvironment has the characteristics of high concentration of GSH.[29] MnO_2 in HMMD is reduced to water-soluble Mn^{2+} by GSH. With the decomposition of MnO_2 nano shell, the pores of

HMCuS were exposed. DOX was then released from HMCuS. MnO_2 was decomposed when HMMD was placed in acidic PBS containing GSH (pH 5.5) (simulating tumor microenvironment). The equation of the reaction is as follows:

$$MnO_2 + 2GSH + 2H^+ \rightarrow Mn^{2+} + GSSG + 2H_2O$$

About 74.9% of DOX was released from HMCuS-MnO_2 nanoparticles within 1h, demonstrating that MnO_2 nano shell coated on the outside of HMCuS could be applied as a "controller" to control the release of DOX. It also can be seen from the TEM in Figure S6A, the outer layer of MnO_2 is consumed in GSH-rich solution, and the structure of HMCuS becomes loose and even collapses. The result of elemental mapping showed that the Mn element in the HMMD nano platform almost disappeared which indicated that GSH reduced MnO_2 to free Mn^{2+} (Figure S6B–E).

In vitro Monitoring of Cellular Uptake, Intracellular Hypoxia and Intracellular ROS Level

To observe the drug delivery of multifunctional nanomaterials and evaluate the tumor-targeting ability of platelet membrane intuitively, we recorded the fluorescence intensity of DOX in 4T1 cells incubated with HMMD and HMMD@PG (Figure 4A). After incubation with HMMD@PG for 1 h, the red fluorescence of DOX was observed in 4T1 cells, indicating that HMMD@PG had been absorbed and internalized into the cells. After incubation with HMMD@PG for 3 h, the red fluorescence of DOX overlapped with the blue fluorescence of the nucleus, indicating that HMMD@PG released DOX and entered the nucleus. Compared with the fluorescence intensity of incubation for 1 h, the fluorescence intensity was significantly enhanced. However, the fluorescence intensity of the HMMD group was weaker than that of the HMMD@PG

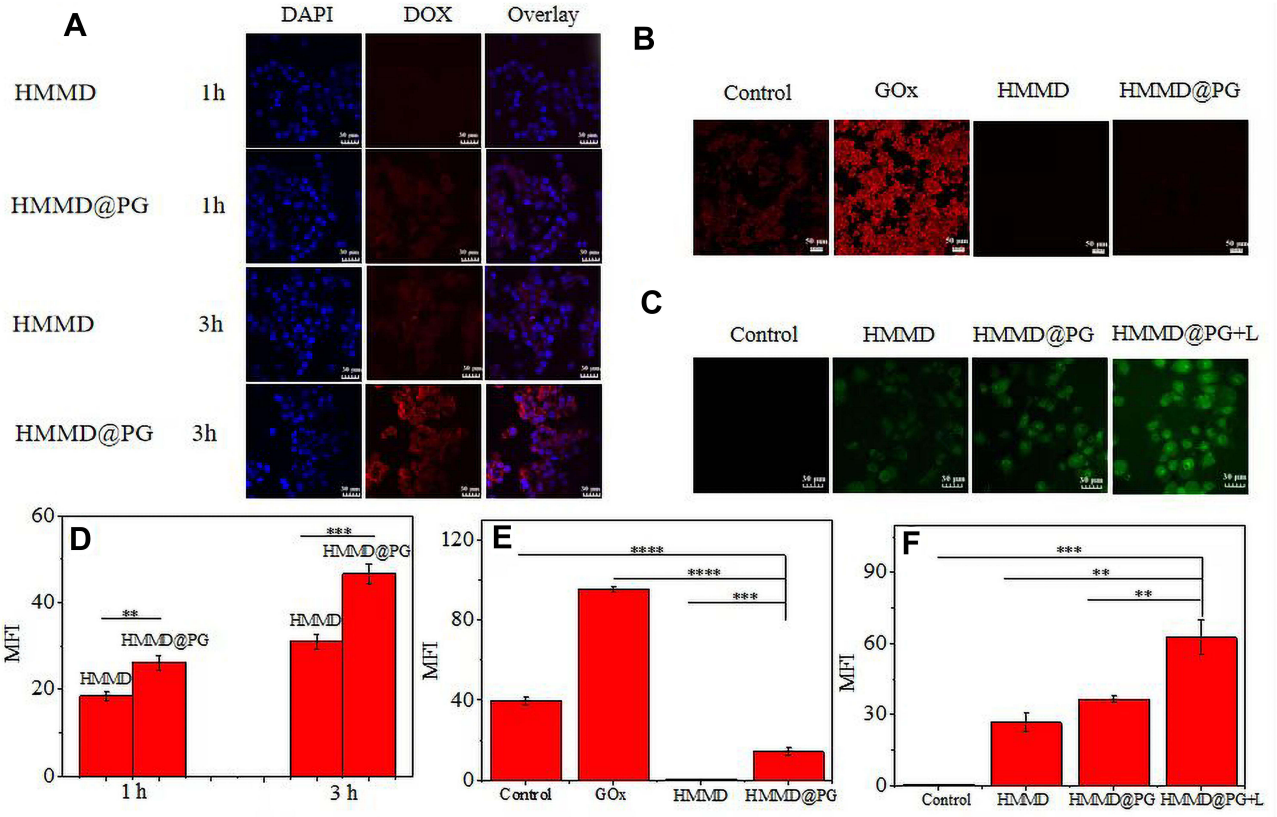

Figure 4 (**A**) CLSM images of 4T1 cells incubated with HMMD and HMMD@PG for 1 h and 3 h. The cell nuclei were stained as blue by DAPI, red was the fluorescence of DOX. Scale bar: 30 μm. (**B**) CLSM images of 4T1 cells incubated with different materials using hypoxia detection probes. Scale bar: 50 μm. (**C**) CLSM images of 4T1 cells incubated with HMMD (100 μg/mL), HMMD@PG (100 μg/mL) and HMMD@PG (100 μg/mL) + L to evaluate the ROS generating capabilities of HMMD@PG in vitro. Scale bar: 30 μm. (**D**) MFI of 4T1 cells co-incubated with different materials on 1h and 3h. (**E**) The analysis of hypoxia levels by MFI in 4T1 cells co-incubated with different materials. (**F**) The analysis of ROS levels by MFI in 4T1 cells co-incubated with different materials. Data were shown as means ± SD (n = 3). ** $p < 0.01$, *** $p < 0.001$, **** $p < 0.0001$.

Abbreviation: MFI, mean fluorescence intensity.

group at the same incubation time. From the results of fluorescence quantification, the fluorescence intensity of the HMMD@PG group was 1.42 and 1.5 times that of the HMMD group, respectively, when the co-incubation time reached 1 h and 3 h (Figure 4D). This result verifies that the encapsulation of PLT membrane enhances the tumor-targeting ability of nanomaterials. This could be attributed to the nesting effect of PLT on tumor cells, and this key role made it a drug carrier for anti-cancer drugs.[30] The increased targeting ability is conducive to enhancing the killing ability to the tumor,[31] which has been verified in the later killing ability of PM encapsulated nanomaterials to tumor cells and the treatment of subcutaneous tumors in mice.

One of the typical characteristics of TME is the lack of oxygen supply. It is reported that MnO_2 can trigger H_2O_2 to generate O_2.[32] In order to study the ability of O_2 production, the intracellular oxygen levels of different samples incubated under hypoxia were monitored by hypoxia fluorescence probe. As shown in Figure 4B and E, compared with other groups, the strongest fluorescence signals were found in 4T1 cells incubated with GOx. This phenomenon could be attributed to the continuous consumption of intracellular oxygen during GOx-mediated glucose oxidation. There were no significant fluorescence signals in the HMMD group, indicating that MnO_2 could decompose the H_2O_2 overexpressed in tumor cells into oxygen, resulting in fluorescence quenching. In contrast, the red fluorescence in 41T cells treated with HMMD@PG was very slight because the prepared nanoreactors could provide oxygen to GOx and alleviate hypoxia in the tumor environment.

To evaluate the efficacy of photodynamic therapy, intracellular ROS generation was detected by a DCFH-DA probe. The probe can be deacetylated by intracellular esterase to be non-fluorescent and then oxidized by ROS into 2',7'-dichlorofluorescein (DCF) that emits green fluorescence.[33] As displayed in Figure 4C, the HMMD group without irradiation showed weak ROS fluorescence originating from the endogenous H_2O_2 in 4T1 cells. A large number of H_2O_2 were generated from the GOx-based glucose oxidation, so the cells incubated with HMMD@PG showed stronger fluorescence. These results substantiated the intracellular cascade reactions between GOx and MnO_2 nanoshell. The cells incubated with HMMD@PG and exposed to irradiation for 5 min showed the strongest fluorescence intensity among all groups. From the results of fluorescence quantification, the fluorescence intensity of HMMD@PG+L group was 2.35 and 1.72 times that of HMMD and HMMD@PG group, respectively (Figure 4F). The introduced MnO_2 nanoshell in the system could decompose the intracellular H_2O_2 and generate a large amount of oxygen, which was favorable for generating ROS during irradiation. The above results demonstrated that HMMD@PG could be used as a photosensitizer for O_2 and ROS generation to alleviate hypoxia and enhance PDT efficacy.

In vitro Cellular Cytotoxicity

Even if the HMCuS nanoparticles concentration is increased to 100 μg/mL, the viability of 4T1 cells still remains above 85% (Figure 5A). This result shows that HMCuS nanoparticles have a high degree of biocompatibility. To test the targeting effect and cancer cell killing ability of the multifunctional nanoplatform, we used the CCK 8 method to evaluate the cytotoxicity of HMMD@PG on the 4T1 cell line. As shown in Figure 5B, compared with the HMMD group, the PLT-GOx membrane-encapsulated HMMD group was significantly more cytotoxic. This is considered to be the credit for the PLT membrane in efficiently delivering GOx to tumor cells using its tumor-targeting function. Thus, it also suggests that tumor starvation treatment by GOx-mediated severed energy supply is highly lethal to 4T1 cells. It was found that the NIR laser significantly improved the heat/chemotherapy effect on 4T1 cells by comparing the NIR pretreatment group and the non-NIR pretreatment group. Compared with the free DOX group, the final experimental group (HMMD@PG + L) showed high superiority in toxicity to tumor cells. The IC50 value of the free DOX group was 3.8 ± 0.09 μg/mL, while that of the HMMD@PG + L group was only 0.96 ± 0.16 μg/mL. The experimental results of CCK8 show that the prepared multifunctional nanoplatform has a significant effect on anti-tumor cells. To observe the killing ability of HMMD@PG on cells more directly, we observed the distribution of living and dead cells by calcium acetyl methyl phosphate (AM) and propidium iodide (PI) staining. Living and dead cells were stained with green and red fluorescence, respectively. As shown in Figure 5C, cells without any treatment grew very well, while cells treated with free DOX observed weak damage. It is worth noting that almost all cells die after HMMD @PG + L treatment, which was considered to be cooperative cancer treatment induced by starvation treatment, PTT, self-supply of H_2O_2, enhanced targeting ability and chemotherapy.

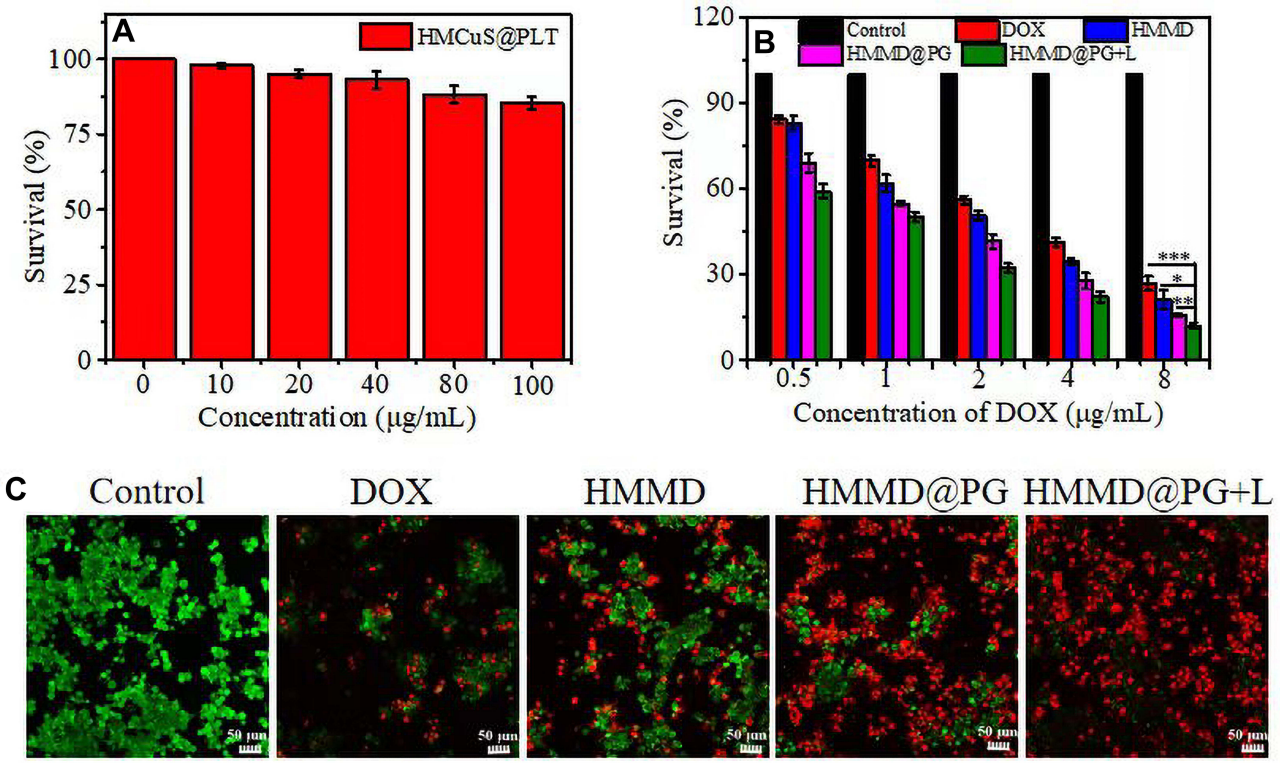

Figure 5 In *vitro* cytotoxicity study. (**A**) Cell viability of 4T1 cells treated with HMCuS@PLT. (**B**) Cell viability of 4T1 cells treated with PBS, DOX, HMMD, HMMD@PG and HMMD@PG + L (1.5 W/cm^2 6min) respectively. (**C**) Fluorescence images of 4T1 cells treated with PBS, DOX, HMMD, HMMD@PG and HMMD@PG + L (1.5 W/cm^2 6min). Scale bar: 50 μm. Data were shown as means ± SD (n = 3). * $p < 0.05$, ** $p < 0.01$, *** $p < 0.001$.
Abbreviation: L, laser.

In vivo Fluorescence Imaging

ICG is the only near-infrared (NIR) dye approved by Food and Drug Administration (FDA), and it has been widely used in imaging contrast agents.[34] The near-infrared dye ICG was loaded into HMCuS in order to track the tumor accumulation behavior of nanoplatforms. The HMCuS-ICG-MnO_2 was characterized by UV-vis, and EE of ICG was also calculated (Figure S7A–B). HMCuS-ICG-MnO_2@PG or free ICG was injected into 4T1 tumor-bearing mice by intravenous injection. The fluorescence distribution in the body was observed using the IVIS spectroscopy system after 0 h, 2 h, 4h, 12 h, 24 h, and 48 h. In vivo tracking results showed that HMCuS-ICG-MnO_2@PG has good tumor accumulation ability, while free ICG is easy to be distributed in other organs (Figure 6A). Over time, free ICG was quickly cleared by the body, and the tumor shows a weak fluorescent signal. However, the fluorescence intensity of the tumors in the HMCuS-ICG-MnO_2@PG treatment group gradually increased, reaching a maximum at 12 h after injection, and still maintained a relatively high level at 48 h after injection. It is worth noting that the fluorescence intensity of the tumors in the HMCuS-ICG-MnO_2@PG group was almost all higher than that in the ICG group within the test time range. The tumor accumulation ability of HMCuS-ICG-MnO_2@PG on 12 h was 11 times higher than that of free ICG (Figure 6B). This consideration is related to the excellent accumulation ability of HMCuS nanoparticles, the targeting effect of PLT membrane on tumors, and the sustained drug release behavior.

In vivo Therapeutic Efficacy

The prepared multifunctional nano-platform with good tumor accumulation and inhibitory ability is expected to become a suitable drug carrier and widely improve the therapeutic effect with minimal side effects.

The tumor suppression effect in vivo was finally explored through the 4T1 xenograft tumor model in order to further evaluate the therapeutic effect of HMMD@PG in vivo. The tumor-bearing nude mice were randomly divided into 5 groups

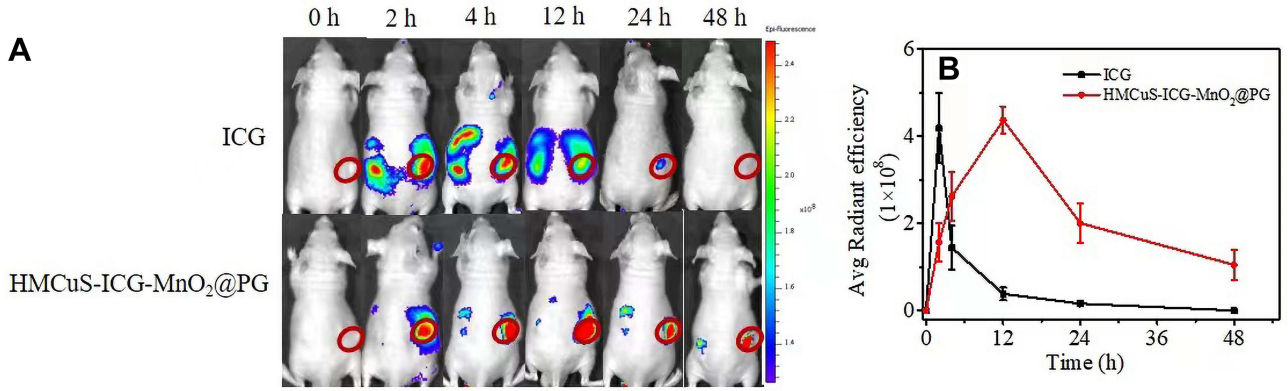

Figure 6 (**A**) Fluorescence distribution at 0 h, 2 h, 4 h, 12 h, 24 h and 48h after injection of ICG and HMCuS-ICG-MnO_2@PG (ICG = 100 μg/mL, 200 μL) in 4T1 tumor-bearing nude mice. (**B**) Region-of-interest analysis of fluorescent intensities from the tumors (green fluorescence represents live cells, red fluorescence represents dead cells). Data were shown as means ± SD (n = 3).

(each group = 5): (I) PBS (control group), (II) DOX, (III) HMMD, (IV) HMMD@PG, (V) HMMD@PG + L. All mice were injected via the tail vein every 2 days, and each mouse was injected 3 times. The mice were sacrificed 14 days later. In order to quantitatively evaluate the treatment effect, the body weight of the mice and the tumor volume were obtained every 2 days during the entire study. The body weight changes of mice in all groups were tiny (Figure 7A), which indicates that the safety of HMMD@PG treatment is higher. However, DOX can cause significant weight loss due to its toxic effects on organisms. The tumor volume (Figure 7B) and relative tumor weight (Figure 7C) of each group explained the therapeutic effect of various treatment methods. The tumor volume increased significantly due to the lack of treatment in the control group. The anti-tumor effect of free DOX and HMMD treatment groups was general. Furthermore, the HMMD@PG group still has a strong tumor

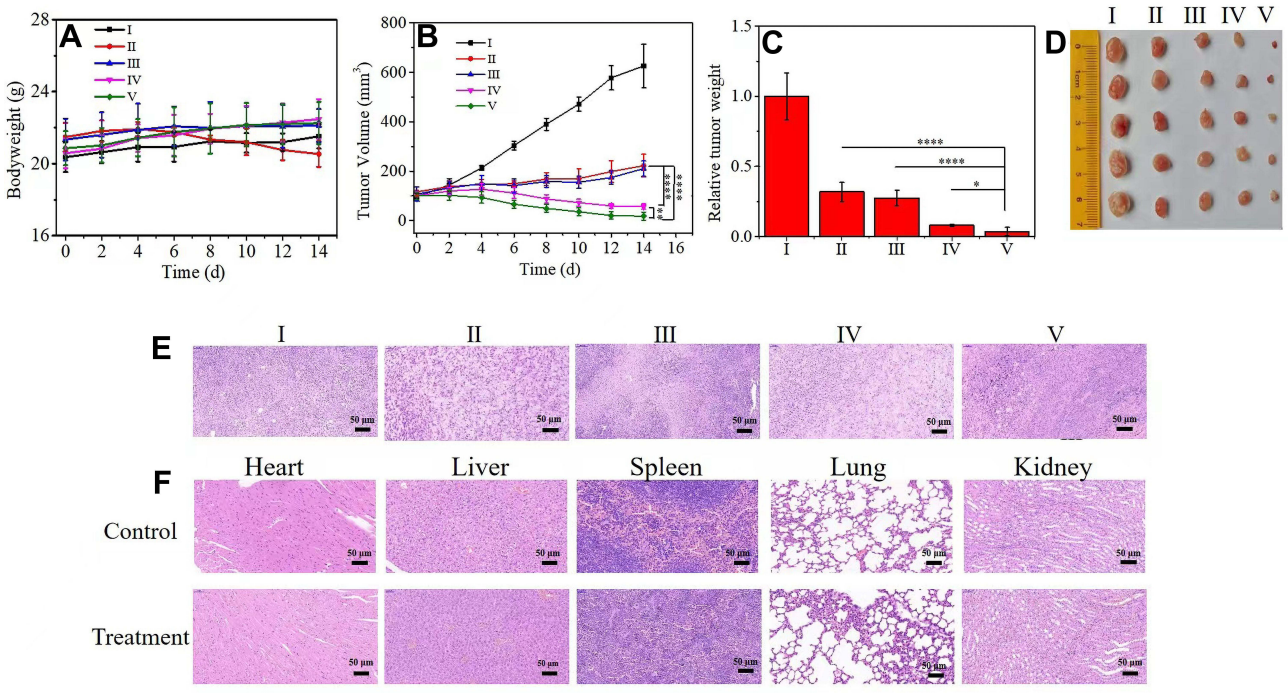

Figure 7 In vivo anticancer study of HMMD@PG +L on 4T1-tumor-bearing mice based on intravenous administration. (I) PBS (control group), (II) DOX, (III) HMMD, (IV) HMMD@PG, (V) HMMD@PG + L. (**A**) Body weight, (**B**) tumor volume, (**C**) relative tumor weight and (**D**) tumor tissue images of 4T1-tumor-bearing mice with different treatments over 14 days. (**E**) H&E staining images of the dissected tumor tissues and (**F**) organs after 14 days of treatment. Scale bar: 50 μm. n = 5, *$p < 0.05$, **$p < 0.01$, ****$p < 0.0001$.

Abbreviation: L, laser.

inhibitory effect, although there is no irradiation to achieve in vivo photothermal treatment, confirming that the presence of PLT-GOx enhances the accumulation of nanoplatforms at tumor sites and GOx-mediated starvation treatment can effectively enhance the anti-tumor effect. Due to the addition of heat/chemotherapy and starvation treatment, the application of HMMD@PG + L can inhibit tumor growth significantly. The corresponding tumor tissue images of mice were further confirmed that HMMD@PG has the highest anti-tumor efficiency with laser assistance (Figure 7D). The HE-stained section images showed that the HMMD@PG + Laser treatment severely destroyed the tumor tissue, while the control group and other treatment groups still had tumor infiltration and prominent tumor characteristics (Figure 7E). Moreover, there is no apparent pathological change after processing the stained images of major organs and tissues, which further illustrates the biological safety of the multifunctional nanosystem (Figure 7F). The results of blood analysis of mice in each group showed that HMMD@PG had no effect on liver and kidney function. (Figure S8A–C).

Conclusion

In summary, we have successfully integrated the multifunction of PLT-GOx and HMCuS -DOX-MnO_2 for the first time to prepare the nanoreactors, HMMD@PG, which can not only improve the therapeutic effect through cascade reaction, but also enhance the tumor accumulation of nanoplatforms by using the tumor-targeting ability of PLT membrane. Here, the PLT membrane coating acts as the guider to guarantee the safe transmission of the GOx and nanoplatforms in normal tissues and enhance nanoreactors accumulation at tumor sites. Glucose and O_2 in the tumor were converted to H_2O_2 under the catalysis of GOx. H_2O_2 is catalyzed by MnO_2 in the nano platform, which can provide O_2 for GOx. High concentrations of GSH in TME are also consumed in this process. The cascade catalytic reactions improved the environment of tumor hypoxia and high concentration GSH. More importantly, the in vivo anti-tumor results and blood analysis also showed the good safety profile of the developed multifunctional nanoplatform. The combined effects of starvation treatment, PTT, and chemotherapy produced by the nanosystem show superior anti-tumor outcomes.

The rational strategy of combining GOx, PLT membrane, and HMCuS-MnO_2 into HMMD@PG represents an effective method to overcome the barriers caused by the TME, which holds great potential to promote the development and translation of GOx.

Acknowledgments

This work was supported by the National Natural Science Foundation of China (22074015), the Key Medical of Jiangsu Province (ZDXKB2016020)(8524006057), and the Key Medical Projects of Jiangsu Province (BL2014078), Jiangsu Social Development Project (BE2018711), Natural Science Foundation of Jiangsu Province (H2019110).

Disclosure

The authors report no conflicts of interest in this work.

References

1. Vaupel P, Multhoff G. Revisiting the Warburg effect: historical dogma versus current understanding. *J Physiol*. 2021;599(6):1745–1757.
2. Huang C, Zhu C, Chen J, et al. Nano-Platelets as an Oxygen Regulator for Augmenting Starvation Therapy Against Hypoxic Tumor. *Front Bioeng Biotechnol*. 2020;8:571993.
3. He T, Xu H, Zhang Y, et al. Glucose Oxidase-Instructed Traceable Self-Oxygenation/Hyperthermia Dually Enhanced Cancer Starvation Therapy. *Theranostics*. 2020;10(4):1544–1554.
4. Shao F, Wu Y, Tian Z, et al. Biomimetic nanoreactor for targeted cancer starvation therapy and cascade amplificated chemotherapy. *Biomaterials*. 2021;274:120869.
5. Fu LH, Qi C, Lin J, et al. Catalytic chemistry of glucose oxidase in cancer diagnosis and treatment. *Chem Soc Rev*. 2018;47(17):6454–6472.
6. Fan W, Lu N, Huang P, et al. Glucose-Responsive Sequential Generation of Hydrogen Peroxide and Nitric Oxide for Synergistic Cancer Starving-Like/Gas Therapy. *Angew Chem Int Ed Engl*. 2017;56(5):1229–1233.
7. Wang J, Huang J, Zhou W, et al. Hypoxia modulation by dual-drug nanoparticles for enhanced synergistic sonodynamic and starvation therapy. *J Nanobiotechnology*. 2021;19(1):87.
8. Fu LH, Qi C, Hu YR, et al. Glucose Oxidase-Instructed Multimodal Synergistic Cancer Therapy. *Adv Mater*. 2019;31(21):e1808325.
9. Wang Q, Zhang X, Huang L, et al. GOx@ZIF-8(NiPd) Nanoflower: an Artificial Enzyme System for Tandem Catalysis. *Angew Chem Int Ed Engl*. 2017;56(50):16082–16085.
10. Wang M, Wang D, Chen Q, et al. Recent Advances in Glucose-Oxidase-Based Nanocomposites for Tumor Therapy. *Small*. 2019;15(51):e1903895.

11. Joseph JP, Harishankar MK, Pillai AA, et al. Hypoxia induced EMT: a review on the mechanism of tumor progression and metastasis in OSCC. *Oral Oncol*. 2018;80:23–32.
12. Ribeiro BFM, Souza MM, Fernandes DS, et al. Graphene oxide-based nanomaterial interaction with human breast cancer cells. *J Biomed Mater Res A*. 2020;108(4):863–870.
13. Xia D, He H, Wang Y, et al. Ultrafast glucose-responsive, high loading capacity erythrocyte to self-regulate the release of insulin. *Acta Biomater*. 2018;69:301–312.
14. Ramadan S, Guo L, Li Y, Yan B, Lu W. Hollow copper sulfide nanoparticle-mediated transdermal drug delivery. *Small*. 2012;8(20):3143–3150.
15. Deng X, Li K, Cai X, et al. A Hollow-Structured CuS@Cu_2 S@Au Nanohybrid: synergistically Enhanced Photothermal Efficiency and Photoswitchable Targeting Effect for Cancer Theranostics. *Adv Mater*. 2017;29:36.
16. Lin X, Fang Y, Tao Z, et al. Tumor-Microenvironment-Induced All-in-One Nanoplatform for Multimodal Imaging-Guided Chemical and Photothermal Therapy of Cancer. *ACS Appl Mater Interfaces*. 2019;11(28):25043–25053.
17. Kunde SS, Wairkar S. Platelet membrane camouflaged nanoparticles: biomimetic architecture for targeted therapy. *Int J Pharm*. 2021;598:120395.
18. Luk BT, Hu CM, Fang RH, et al. Interfacial Interactions Between Natural RBC Membranes and Synthetic Polymeric Nanoparticles. *Nanoscale*. 2014;6:2730–2737.
19. Traverso N, Ricciarelli R, Nitti M, et al. Role of glutathione in cancer progression and chemoresistance. *Oxid Med Cell Longev*. 2013;2013:972913.
20. Wang Y, Zhang S, Wang J, et al. Ferrocene-containing polymersome nanoreactors for synergistically amplified tumor-specific chemodynamic therapy. *J Control Release*. 2021;333:500–510.
21. Liu Y, Ai K, Liu J, et al. Dopamine-melanin colloidal nanospheres: an efficient near-infrared photothermal therapeutic agent for in vivo cancer therapy. *Adv Mater*. 2013;25(9):1353–1359. doi:10.1002/adma.201204683
22. Zhu H, Wang J, Wu D. Fast synthesis, formation mechanism, and control of shell thickness of CuS hollow spheres. *Inorg Chem*. 2009;48 (15):7099–7104.
23. Zhang M, Xing L, Ke H, et al. MnO_2-Based Nanoplatform Serves as Drug Vehicle and MRI Contrast Agent for Cancer Theranostics. *ACS Appl Mater Interfaces*. 2017;9(13):11337–11344.
24. Guo W, Chen Z, Chen J, et al. Biodegradable hollow mesoporous organosilica nanotheranostics (HMON) for multi-mode imaging and mild photo-therapeutic-induced mitochondrial damage on gastric cancer. *J Nanobiotechnology*. 2020;18(1):99.
25. Xu JT, Han W, Yang PP, et al. Tumor Microenvironment-Responsive Mesoporous MnO2-Coated Upconversion Nanoplatform for Self-Enhanced Tumor Theranostics. *Adv Funct Mater*. 2018;28:1803804.
26. Bansal A, Simon MC. Glutathione metabolism in cancer progression and treatment resistance. *J Cell Biol*. 2018;217(7):2291–2298.
27. Lin LS, Song J, Song L, et al. Simultaneous Fenton-like Ion Delivery and Glutathione Depletion by MnO_2 -Based Nanoagent to Enhance Chemodynamic Therapy. *Angew Chem Int Ed Engl*. 2018;57(18):4902–4906.
28. Gu D, An P, He X, et al. A novel versatile yolk-shell nanosystem based on NIR-elevated drug release and GSH depletion-enhanced Fenton-like reaction for synergistic cancer therapy. *Colloids Surf B Biointerfaces*. 2020;189:110810.
29. Ni D, Jiang D, Valdovinos HF, et al. Bioresponsive Polyoxometalate Cluster for Redox-Activated Photoacoustic Imaging-Guided Photothermal Cancer Therapy. *Nano Lett*. 2017;17(5):3282–3289.
30. Dovizio M, Ballerini P, Fullone R, et al. Multifaceted Functions of Platelets in Cancer: from Tumorigenesis to Liquid Biopsy Tool and Drug Delivery System. *Int J Mol Sci*. 2020;21(24):9585.
31. Sounni NE, Noel A. Targeting the tumor microenvironment for cancer therapy. *Clin Chem*. 2013;59(1):85–93.
32. Huang J, Huang Y, Xue Z, et al. Tumor microenvironment responsive hollow mesoporous Co_9S_8@MnO_2-ICG/DOX intelligent nanoplatform for synergistically enhanced tumor multimodal therapy. *Biomaterials*. 2020;262:120346.
33. Fu LH, Wan Y, Qi C, et al. Nanocatalytic Theranostics with Glutathione Depletion and Enhanced Reactive Oxygen Species Generation for Efficient Cancer Therapy. *Adv Mater*. 2021;33(7):e2006892.
34. Egloff-Juras C, Bezdetnaya L, Dolivet G, et al. NIR fluorescence-guided tumor surgery: new strategies for the use of indocyanine green. *Int J Nanomedicine*. 2019;14:7823–7838.